

## Correlation of the LeTID amplitude to the Aluminium bulk concentration and Oxygen precipitation in PERC solar cells



Matthias Wagner\*, Franziska Wolny, Melanie Hentsche, Andreas Krause, Lamine Sylla, Frieder Kropfgans, Malte Ernst, Robert Zierer, Paul Bönisch, Petra Müller, Nicole Schmidt, Viktor Osinniy, Hans-Peter Hartmann, Raik Mehnert, Holger Neuhaus

*Solar World Industries GmbH, Martin-Luther-King-Str. 24, 53175 Bonn, Germany*

### ARTICLE INFO

**Keywords:**

Light induced degradation  
PERC solar cell  
Bulk metal contamination  
Czochralski-grown silicon

### ABSTRACT

We performed an extensive study of light induced degradation experiments in PERC solar cells made of Boron doped Cz Silicon material from several experimental crystals. Strong LeTID (Light and Elevated Temperature Induced Degradation) amplitudes were found in cells originating from the top and tail part of the crystals. A statistical analysis reveals a strong correlation to the bulk concentration of Aluminium in cells originating from wafers close to the tail. Close to the top, the LeTID effect is strongly enhanced whenever Oxygen precipitation occurs in the cell process.

### 1. Introduction

In recent years, Silicon solar cell efficiency in industrial processes has increased to new record levels, exceeding 22% [1,2]. This was made possible by a switch from the previous standard technology using an Aluminium Back Surface Field (Al-BSF) process to the so-called PERC technology (Passivated Emitter and Rear Solar Cell). In the Al-BSF process, recombination at the interface between Silicon bulk and the rear metallization was the dominant loss mechanism. PERC solar cells, on the other hand, are now limited to a larger extent by the electrical quality of the front (emitter and passivation) and by recombination processes in the Silicon bulk. Recombination active defects, either originating from crystal growth, introduced during cell processing or being activated by illumination, therefore cause a stronger relative decrease in cell efficiency than in Al-BSF cells.

Light induced degradation (LID) in Silicon solar cells was already observed in the 1970s [3]. Since a correlation of this effect to both the Boron and the Oxygen concentration was observed [4], the defect causing this degradation was called “Boron-Oxygen defect”, even though the exact defect configuration has not been determined to date. In order to distinguish this kind of degradation from the other ones discussed in the following, we use the term “B-O LID” for this effect. Later, Möller and Lauer suggested that Oxygen was not directly involved in the “Boron-Oxygen defect”. They suggested an “Asi-Si<sub>i</sub>” configuration, where “A” stands for the possible acceptors Aluminium, Boron, Gallium, and Indium [5,6]. This complex defect consists of an

acceptor atom on a substitutional Silicon site, accompanied by a displaced Silicon atom on a nearby interstitial site.

When the PERC process sequence started to become industrially feasible, Ramspeck et al. observed an unexpectedly high degradation upon illumination at moderately increased temperature (75 °C) [7]. This effect was particularly strong in cells made of multicrystalline or mono-like (QuasiMono) wafer material. The Oxygen concentration in these wafer types is considerably lower than in Czochralski (Cz) material, which made it unlikely that this degradation was the same as the B-O LID described above. Due to its particular features, and in order to distinguish it from the B-O LID effect, Kersten et al. introduced the name LeTID (Light and elevated Temperature Induced Degradation) for this phenomenon [8]. It was originally believed that LeTID only occurs in multicrystalline material. Later it was detected also in solar cells made from Cz crystals [9]. It is of major importance to understand the origin of this phenomenon, since it is, in some respects, more severe than the well-known B-O LID. In particular, its regeneration behavior is more unfavorable.

In order to identify the root cause for the LeTID phenomenon, both experimental and theoretical investigations have been published. It was shown that LeTID in multicrystalline material only occurs when a passivation layer is present on at least one wafer surface during the fast firing step, which is necessary for contact formation to the metallization [10]. Vargas et al. interpreted this finding as related to the amount of Hydrogen released from the passivation layers into the wafer bulk during the fast firing [11]. By using both injection dependent and

\* Corresponding author.

E-mail address: [mtwagnerfg@web.de](mailto:mtwagnerfg@web.de) (M. Wagner).

temperature dependent lifetime spectroscopy, Morishige et al. could narrow down the possible values for the relevant defect parameters after degradation in LeTID dominated multicrystalline material. By comparing these to literature values, they suggested that LeTID may be related to the presence of Tungsten [12]. Later on, Niewelt et al. found “denuded zones” of reduced LeTID amplitude in the vicinity of grain boundaries in multicrystalline material. These denuded zones are assumed to originate from a gettering effect of the grain boundaries on one of the elements involved in the defect underlying the LeTID effect. From the width of the denuded zone, they could draw conclusions about possible candidates, since the solubilities and diffusivities of most of the relevant metallic impurities at the process temperatures during cell processing are known. Based on this, it was suggested that the LeTID phenomenon may be related to Cobalt contamination [13].

It has been shown by several groups that the amount of degradation due to the LeTID phenomenon can be influenced by variations in cell processing, in particular by optimization of the fast firing profile [14]. In our screening of solar cells produced from a large number of different experimental B-doped Cz crystals, we find strongly varying LeTID amplitudes for identical cell processing details, in particular when fired using identical profiles. This implies that the origin of the LeTID phenomenon lies in properties of the Cz material itself. No attempt was made to vary the Hydrogen content in our solar cells. All cells were coated with dielectric layers on both sides using standard process parameters in all cases. We can, thus, assume that the Hydrogen content is comparable in all experiments. No conclusions about the involvement of Hydrogen in formation of the LeTID phenomenon are possible based on our studies.

The price for the raw Silicon wafer constitutes a significant share of the final price for a PV module. In a highly competitive environment, all processes have to be continuously optimized concerning their costs. Before introducing cheaper components (e.g. Silicon feed stock, graphite parts in Czochralski furnaces, crucibles, ...) into production, the impact of this process change on wafer quality has to be evaluated. For this purpose, it is very important to quantify critical concentrations of relevant impurity elements, which can be tolerated. Another important cost saving measure is to pull multiple crystals out of the same crucible by recharging after each pull. Up to three crystals were pulled consecutively in our experimental program and evaluated concerning their efficiency potential and their degradation behavior.

In previous experiments, we repeatedly and reproducibly found a systematic variation of the LeTID amplitude along the crystal length. Since the wafers were randomized prior to and during cell processing, a systematic influence of the cell processing, leading to the observed behavior, could be ruled out. The LeTID defect, or one of its constituents or precursors, has to consist of defects already present in the grown Cz crystal.

The major defects in electronic grade Cz material are related to Oxygen and to crystal defects originating from a vacancy or self-interstitial supersaturation. Whether a Cz crystal contains mainly vacancies or self-interstitials, is determined by the value of the so-called Voronkov coefficient  $v/G$ , where  $v$  is the pulling speed and  $G$  the thermal gradient across the growth front [15]. The Oxygen content can be altered by measures like varying the Argon flow rate, the crystal rotation or the process pressure. Systematically changing these parameters, we assumed to be able to influence the LeTID behavior.

Alternatively, we suspected that some kind of impurity is responsible for LeTID. This was based on the observation of increasing

LeTID amplitude towards the tail and from 1st to 3rd pull (see below). It is also in line with part of the literature cited above. In order to test this hypothesis, we varied the feedstock, e.g. by increasing the remelt fraction or using 100% prime poly material.

## 2. Experimental details

### 2.1. Sample preparation

In our experimental program we grew Boron-doped Cz crystals with strongly varying properties. The more than 40 growth runs can roughly be grouped as aiming at:

- (i) Varying the concentration of the intrinsic defects (Silicon interstitials or vacancies) in a systematic way;
- (ii) Reducing the Oxygen concentration;
- (iii) Reducing the concentration of relevant metallic contaminations.

In (i) we varied both the pulling speed and the temperature gradient at the growth front (aiming at varying Voronkov coefficients, thus introducing different amounts of Silicon interstitials or vacancies, respectively [15]). Examples for measures to influence the Oxygen concentration (ii) are: Increased gas flow rate, reduced process pressure or changes in the hot-zone design. For (iii), we compared crystals grown from 100% prime poly feedstock to different feedstock compositions. In addition, critical components in the Cz furnaces were exchanged, in particular we used crucibles from different vendors and varying quality. Up to three crystals were pulled consecutively from the same crucible.

We measured the concentration of relevant impurities at several positions in our crystals. Each complete crystal was cut into four sections with a length of typically 500 mm. The top-most section is called “A”, the tail-most one “D”. We cut thicker slices from the very top and very tail of the first and last section. The nomenclature is visualized in Fig. 1.

The resistivity of the samples was determined by the Four-Point-Probe technique; both initially and after an appropriate thermal donor anneal (720 °C, 120 s in an RTP furnace). The Oxygen and Carbon concentrations were obtained from Fourier Transform Infrared Spectroscopy (FTIR) measurements.

Metal impurity concentrations were determined using ICP-MS (Inductively Coupled Plasma Mass Spectroscopy). For this purpose, small pieces were cut from the thick slices close to the center position. They were carefully surface etched several times (total etch removal at least 10 μm) in order to remove possible surface contamination contributions. After that, the pieces of Silicon were completely dissolved in a gaseous HF/HNO<sub>3</sub>-atmosphere in order to receive a matrix reduced residue, which is re-dissolved for ICP-MS measurement. In this technique, the measurement effort increases with every element which has to be screened. Based on the experience obtained in previous experiments we focused on the following elements: Fe, Cr, Ni, V (elements contained in stainless steel parts), Cu, Ti, Zn, Al. In some cases, also the concentrations of Mo, W, Pb and Co were determined. However, for these elements the available data is not sufficient for a statistical analysis.

The entire crystals (except the thick slices) were wafered in an industrial wafering process. They received a special laser marking, coding their vertical position in the crystal. Then they were processed into Cz-PERC cells using an industrial cell process. Typically, we achieved cell



**Fig. 1.** Naming of the crystal sections and position of the thick slices used for determination of the impurity concentrations.

efficiencies of approximately 21%, the open circuit voltage was in the range of (0.66 – 0.67) V.

Representative cells resulting from wafers at well-defined vertical positions were chosen for characterization. IV curves at standard testing conditions of these cells were measured initially, and after 1 h, 4 h, 7 h, 25 h, 75 h and 163 h of illumination. The illumination intensity was equivalent to ~0.5 suns (~500 W/m<sup>2</sup> of an AM1.5 solar spectrum), temperature was actively held constant at 75 °C.

## 2.2. Quantifying LeTID

In solar cells made of Cz material, both the B-O LID and LeTID may occur simultaneously. In order to separate the effects, one has to make use of the different dependencies of degradation and regeneration amplitude on temperature and illumination intensity.

The B-O LID leads to an efficiency loss of (3–5)%<sub>rel</sub>, depending on the Boron and Oxygen concentrations c[B] and c[O], under illumination. Moderately increasing the temperature during illumination leads to a faster degradation rate, while the maximum power loss is found to be independent of temperature. Increasing the temperature further and using a stronger light intensity results in the onset of the so-called regeneration process [16]. At 160° and 1 sun (1000 W/m<sup>2</sup>) illumination intensity, the original cell efficiency is restored within less than 30 min. Since this process is thermally activated, the regeneration time increases exponentially when using lower temperatures. Under our standard degradation conditions (75 °C, 0.5 suns), it takes approximately three days (75 h) to complete the regeneration.

The LeTID effect can reduce the cell power more drastically than the B-O LID mechanism. Efficiency losses up to 15%<sub>rel</sub> have been reported. Moderately increasing the temperature speeds up the process. However, contrary to the B-O LID, the maximum power loss also increases with temperature. A regeneration process is also observed for LeTID affected cells, but it requires higher temperatures and stronger illumination. Therefore, at (75 °C, 0.5 suns) regeneration of the LeTID contribution

can be neglected even after one week of illumination.

Fig. 2 shows degradation curves for the relevant cell parameters  $\eta$  (efficiency), FF (fill factor),  $V_{oc}$  (open circuit voltage) and  $I_{sc}$  (short circuit current) at two different illumination conditions: (80 °C, 0.4 suns; open symbols) and (30 °C, 0.1 suns; filled symbols). The red curves originate from cells dominated by the B-O LID, green curves from cells affected mainly by LeTID, and the black curves indicate a mixed case, containing contributions from both B-O LID and LeTID.

In the B-O LID case, the major contribution to the efficiency degradation originates in a decrease of FF, followed by  $V_{oc}$  and  $I_{sc}$ . Contrary to that, LeTID affects  $I_{sc}$  most strongly, followed by  $V_{oc}$  and FF. No regeneration is observed in the LeTID dominated cells at (80 °C, 0.4 suns) until the end of the degradation cycle (one week). But it is also apparent that the LeTID amplitude has not yet reached its saturation value. However, from the shape of the curve we can assume that the largest part of the LeTID degradation occurs within the first 150 h at these conditions.

At (30 °C, 0.1 suns) the LeTID amplitude is weak. Therefore, the degradation curve of the cells in the mixed case under these conditions resembles the curve in typical B-O LID dominated cells. The B-O LID is completely regenerated after 100 h at (80 °C, 0.4 suns).

Fig. 3 compares the situation at (80 °C, 0.4 suns) in the three typical cases. For cells in the mixed case, the situation after one week (163 h) of degradation at (75 °C, 0.5 suns), which is basically identical to (80 °C, 0.4 suns), can be summarized as follows (see red circles in Fig. 3):

- The B-O LID component is completely regenerated;
- The largest part of the LeTID degradation is completed;
- Regeneration of the LeTID component has not yet started.

For these reasons, the degradation amplitude under these conditions is found to be a very good measure for the LeTID strength. In the following, we will use these as standard conditions for quantifying LeTID separately from the B-O LID.

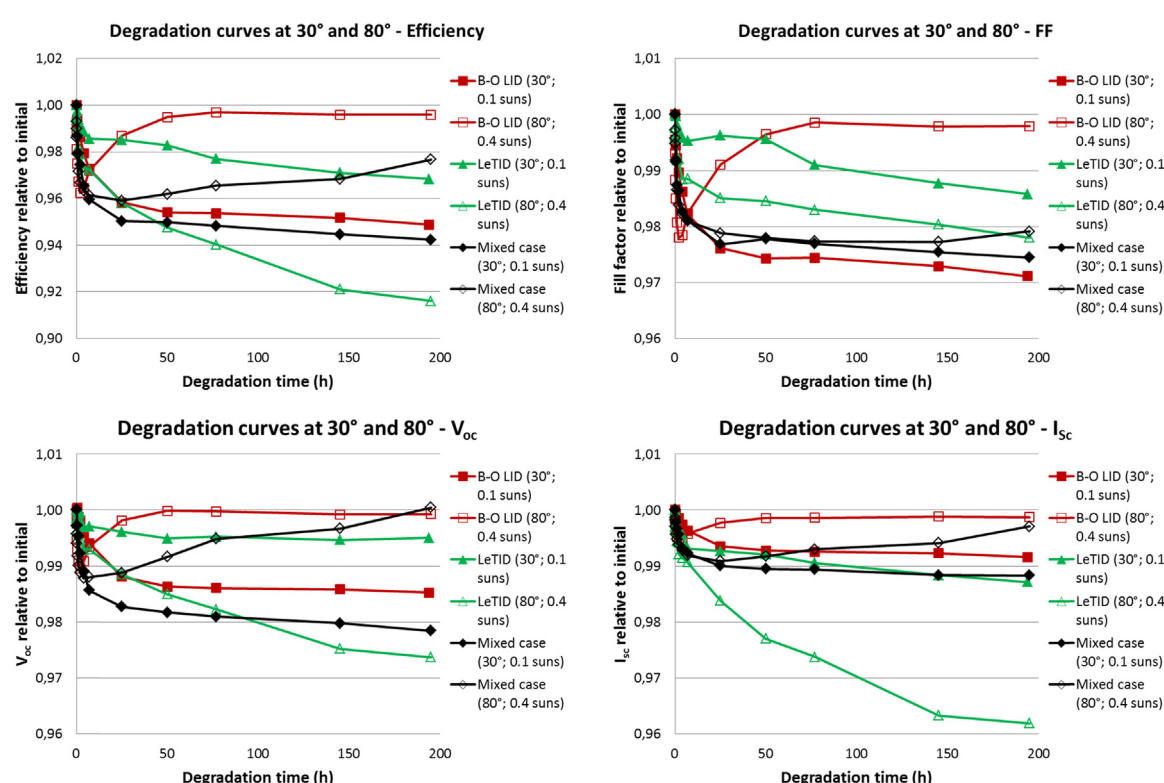


**Fig. 2.** Degradation curves for the relevant cell parameters at (30 °C, 0.1 suns; filled symbols) and (80 °C, 0.4 suns; open symbols) for cells affected by the B-O LID only (red), the LeTID mechanism only (green) and in the mixed case (black).

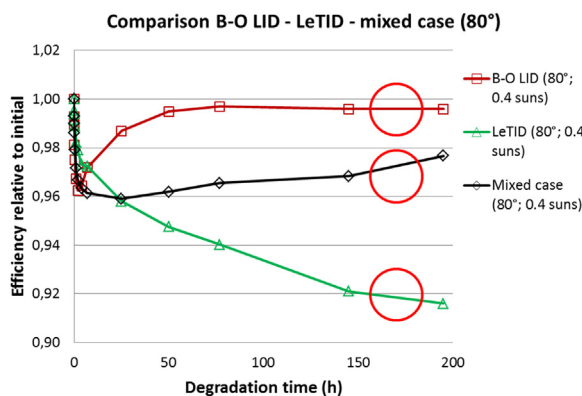


**Fig. 3.** Comparison of the degradation curves at (80 °C, 0.4 suns) in the three typical cases.

### 2.3. Enhancing Oxygen precipitation during cell processing

The solubility of Oxygen in Silicon crystals decreases during cool down from the growth temperature. At some temperature, the solubility falls below the Oxygen concentrations often found in Czochralski grown crystals (typically  $(5 \dots 14) \times 10^{17} \text{ cm}^{-3}$ ). At this point, there is a thermodynamic driving force for precipitation of Oxygen atoms. However, for this process to occur the mobility of Oxygen atoms has to be still high enough in order to reach precipitation sites. If this is not the case, a supersaturation of Oxygen can be maintained at room temperature or moderately enhanced temperatures.

When such wafers are heated during cell processing, Oxygen precipitation can set in, if (i) the Oxygen concentration is sufficiently high, and (ii) if there exist nucleation sites at which precipitation starts. It has been shown that the number of Oxygen precipitates, which grow during high temperature processing in a temperature range of  $\sim (800\text{--}950)^\circ\text{C}$ , is strongly enhanced by a “nucleation step”. This nucleation step consists of an annealing in air at  $(550\text{--}650)^\circ\text{C}$  for several minutes up to several hours [17].

Whether the precipitation nuclei really grow into full sized precipitates during high temperature annealing, depends on the temperature ramp-up speed to the maximum temperature. In the theory of Ostwald ripening, there exists for each temperature a critical precipitate radius  $r_c$ . If, at a given temperature, an existing precipitate has a radius smaller than  $r_c$ , it will dissolve. If, on the other hand, its radius is already larger than  $r_c$ , it will continue growing. This critical radius increases with increasing temperature [17]. As a consequence, if the temperature ramping speed is high enough, all pre-existing precipitates will dissolve because they cannot grow fast enough to avoid dissolving at some point. However, for slow enough ramping speed, a large part of the pre-existing precipitates will continue growing during the entire high temperature processing.

We designed two experiments in order to test the influence of Oxygen precipitation on both the initial cell efficiency and on the LID or LeTID behavior of PERC solar cells:

- Experiment 1: Wafers from section A of a crystal known to be moderately strongly affected by LeTID were processed into PERC solar cells. Prior to the first high temperature process step ( $\text{POCl}_3$  diffusion), these wafers received additional annealing treatments in air (see Table 1). The effect of these treatments on initial cell efficiency and degradation behavior was monitored.
- Experiment 2: Wafers from different positions, purchased from several vendors, were processed into PERC solar cells. The temperature profiles of the high temperature process steps (diffusion and emitter oxidation) were varied (see Table 2). Again, the effect on initial cell efficiency and degradation behavior was recorded.

**Table 1**  
Annealing times and temperatures in Experiment 1.

Annealing temperature (°C)	Annealing time (min)
850	5, 30, 180
600	5, 30, 180

**Table 2**  
Process variations in Experiment 2.

Group	Process variation
DIF slow cool	4 × slower temperature ramp-down speed after $\text{POCl}_3$ diffusion
DIF slow heat	4 × slower temperature ramp-up speed in $\text{POCl}_3$ diffusion
OXI slow cool	4 × slower temperature ramp-down speed after emitter oxidation
OXI slow heat	4 × slower temperature ramp-up speed in emitter oxidation
Ref	Standard PERC process

In both experiments, all wafers received a special laser marking. At process start, the position of these wafers in the batch was randomized. By reading out the laser marking before the process variations, the respective wafers were collected from the batch and received the intended process variations. Afterwards the entire batch was randomized again and processed together. The finished PERC solar cells were then sorted according to their laser marking. Any systematic error due to process differences other than the intended ones can, thus, be ruled out.

## 3. Results

### 3.1. Position dependent degradation curves

Depending on the position of the wafer in the grown crystal, the shape of the degradation curves changes significantly. Four examples are shown in Fig. 4. In these, and in all following charts containing degradation curves, the blue curve marked “control group” consists of solar cells which are stored in dark. Their IV data is recorded immediately before measuring the actual cells under test. The results of the “control group” thus serve as a test for the stability of the measurement system.

In Growth Run 01\_a, most cells are dominated completely by the B-O LID as described above. Only the two cells originating from wafers closest to the tail regenerate slower than the rest of the cells, indicating that they may contain a small LeTID contribution. Similarly, the cells made of wafers from section A in Growth Run 02\_a regenerate slower than expected from B-O LID behavior, but eventually they reach approximately 99% of their original efficiency again. The cell closest to the seed has a very strong LeTID component. In section D, all cells from this crystal are LeTID dominated, the LeTID amplitude increases continuously towards the tail. The crystals from Growth Run 02\_b and Growth Run 14, finally, show very strong LeTID behavior over the entire crystal length.

Examining a large number of experimental crystals, we typically observe the following (Fig. 5 left):

- Almost complete regeneration after one week of illumination at  $(75^\circ\text{C}, 0.5 \text{ suns})$  in section A;
- Increasing LeTID component towards the tail;
- Increasing LeTID component in tail part for 2nd and 3rd pull grown in identical crucible.

However, in some cases rather strong LeTID amplitudes are also found in the top section (section A) of crystals (Fig. 5 right).

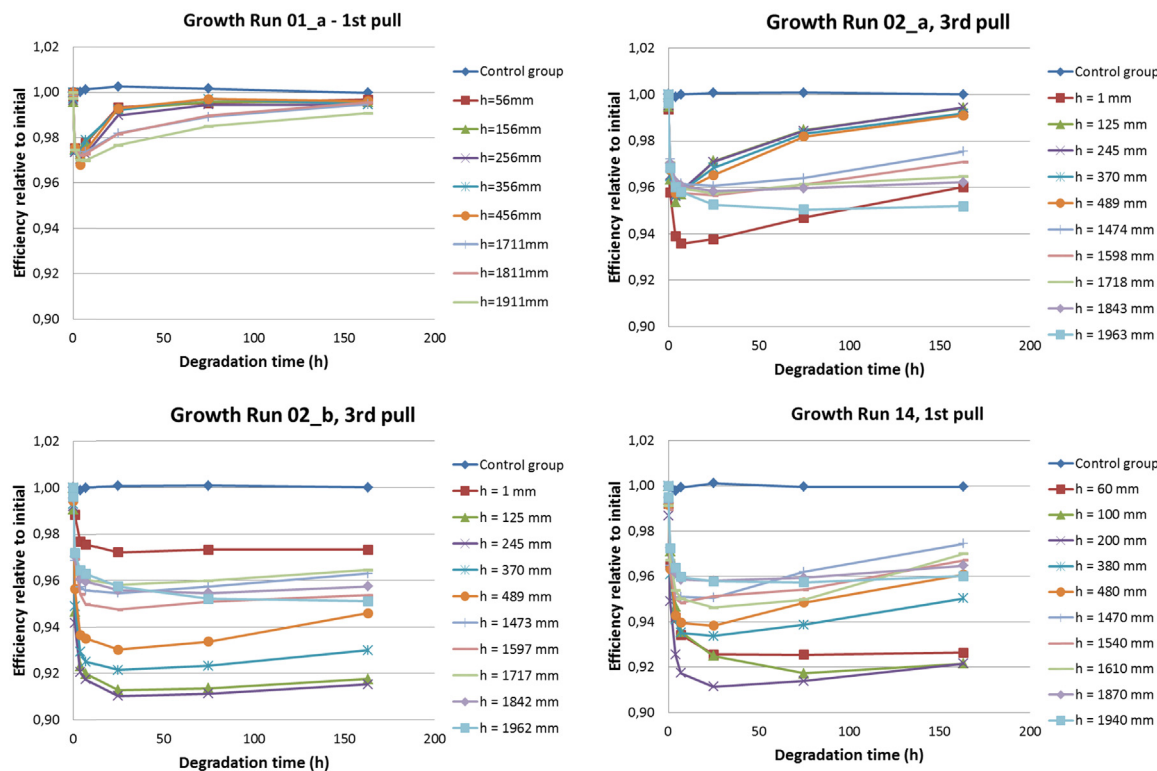


**Fig. 4.** Position dependent degradation curves for Cz-PERC solar cells produced from wafers of four different crystals. Data in the legend indicates the position of the underlying wafer in the crystal, measured from the top of the usable crystal.

### 3.2. Impurity distribution along crystal length

As described above, we determined the concentration of the relevant impurities at four different positions along the crystal length:

- At the very top of section A, i.e. closest to the seed (sample A1);
- At the tail of section A, ~500 mm from the top of the crystal (sample A2);
- At the top of section D, ~1500 mm from the top of the crystal (sample D1);
- At the very tail of section D, i.e. closest to the tail of the entire

crystal (sample D2).

The concentration of the major impurities Oxygen and Carbon was measured using FTIR. In this technique, only impurity atoms residing on specific sites in the crystal can be detected: Oxygen on an interstitial site ( $O_i$ ) and Carbon on a substitutional site ( $C_s$ ). Complex defects like Oxygen precipitates or SiC particles are ignored.

The metal impurities, on the other hand, were determined using ICP-MS. In this technique, the total impurity amount is quantified, independent of the defect configuration in the crystal.

When a certain amount of impurity atoms is already dissolved in the

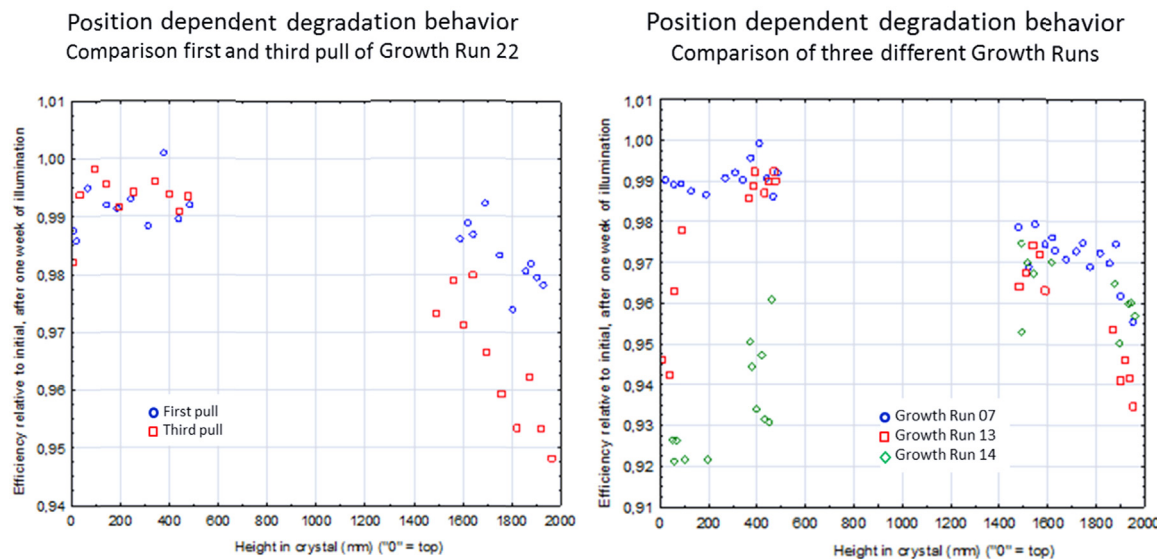


**Fig. 5.** Position dependent degradation amplitude after one week of illumination at (75 °C, 0.5 suns) in a typical experiment (left). In some cases, strong LeTID is found close to the top or even in the entire crystal (right).

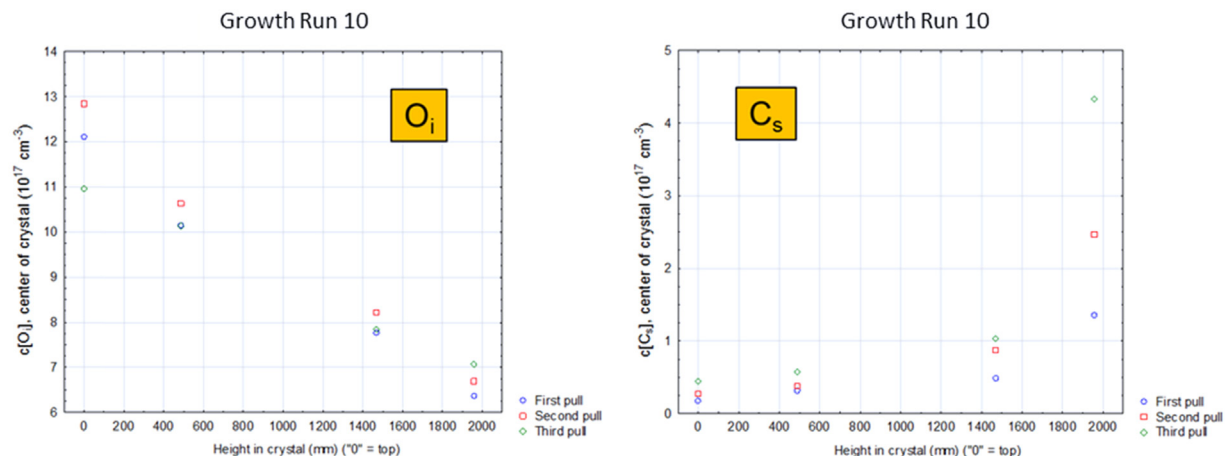


**Fig. 6.** Distribution of interstitial Oxygen and substitutional Carbon, determined by FTIR, along the crystal length for three pulls from the same crucible in a typical experiment.

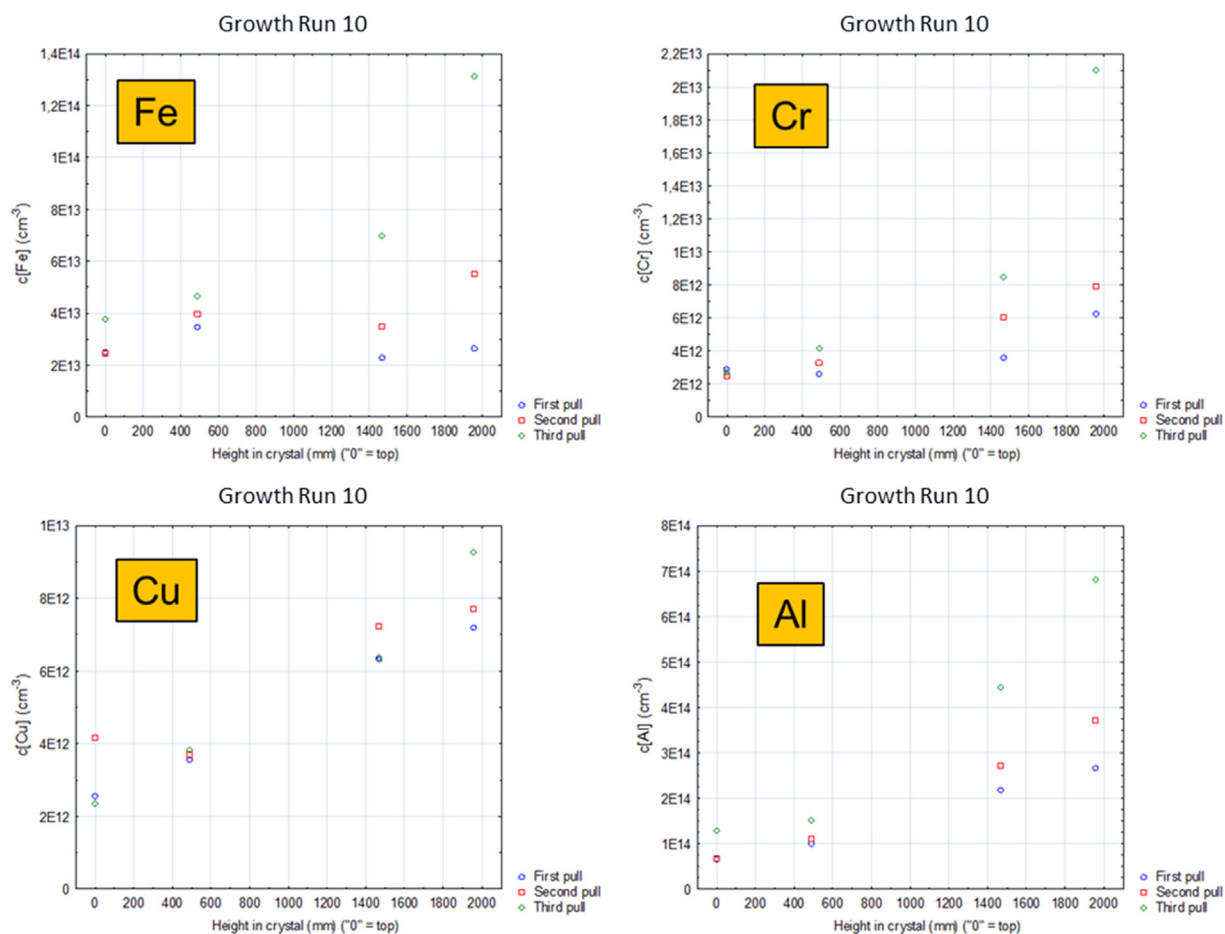


**Fig. 7.** Distribution of iron, chromium, copper and aluminium, determined by ICP-MS, along the crystal length for three pulls from the same crucible in a typical experiment.

melt prior to crystallization, the distribution in the crystal is described by the Scheil equation. Since the solubility in the melt is typically higher than in the solid, the impurity content accumulates in the melt. Consequently, the impurity concentration in the crystal increases towards the tail in a characteristic way. We found this Scheil-like distribution mainly for Carbon and for the dopant Boron, which is intentionally introduced into the melt. There are significant deviations for the metal impurities. Nevertheless, we find increasing metal concentrations from top to tail, and from 1st to 3rd pull in most cases. In

Fig. 7, the distribution of the major metallic impurities Fe, Cr, Cu and Al along the crystal length is displayed.

Oxygen behaves differently than the other elements (Fig. 6). The decreasing concentration from top to tail originates from the fact that this impurity is added continuously to the melt by slow dissolution of the quartz crucible. In the beginning of the growth process, a larger fraction of the crucible wall is in contact with the silicon melt. This leads to higher Oxygen content towards the seed. No significant variation of the Oxygen concentration from 1st to 3rd pull was found in our

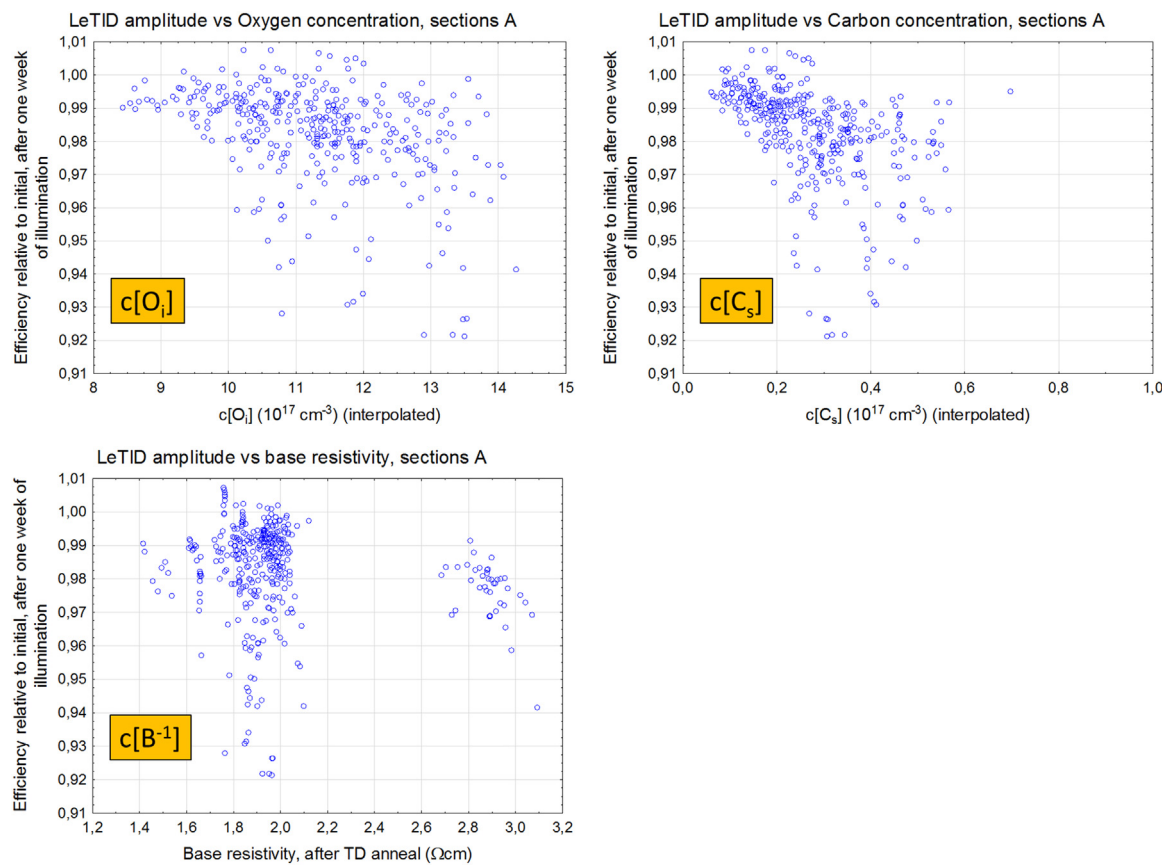


**Fig. 8.** Correlation of the LeTID amplitude (degradation amplitude after one week at (75 °C, 0.5 suns)) to the concentration of Oxygen and Carbon, and to the base resistivity in the sections A of the investigated crystals.

experiments.

As apparent from our sampling scheme and from Figs. 6 and 7, there are no directly determined impurity concentration values for each processed solar cell. On the other hand, there are no abrupt changes in these concentrations along the crystal length. We, therefore, used linear interpolation of the relevant concentrations between A1 and A2 in section A, and between D1 and D2 in section D. According to its position in the grown crystal, each solar cell was, thus, assigned an interpolated value of these concentrations. This allowed us to correlate the degradation behavior of all cells to the impurity content, being aware that the assigned values may deviate from the actual values.

### 3.3. Correlation of the LeTID amplitude to impurity concentrations

#### 3.3.1. Results from section A (close to the top)

In Figs. 8 and 9, the LeTID amplitude is shown in dependence of the interpolated impurity concentrations as described above for solar cells originating from section A of our experimental crystals.

Oxygen concentrations in sections A are always rather high, at least  $8 \times 10^{17} \text{ cm}^{-3}$ . However, for  $c[\text{O}_i] < 10 \times 10^{17} \text{ cm}^{-3}$ , we find negligible LeTID amplitudes. Above this critical concentration, both moderate and high LeTID is found, with an increasing trend towards higher Oxygen concentration.

Carbon concentrations are relatively low close to the top. Nevertheless, increasing  $c[\text{C}_s]$  apparently enhances LeTID. No dependence of the LeTID amplitude on the base resistivity, i.e. the Boron concentration is found.

The highest concentrations concerning metal impurities were found for the elements Al, Cr, Cu, Fe, Ni and Ti. The concentrations of W and Co, when determined, were always low, typically in the range of  $(10^{11} - 10^{12}) \text{ cm}^{-3}$ . These elements are not considered in the following. Fig. 9

shows that there is a general trend to higher LeTID amplitudes for all metallic impurities. However, low LeTID amplitudes even at the highest detected concentrations are apparently possible for all elements except Aluminium.

No direct strong correlation to any impurity is found by simply plotting the LeTID amplitude vs the various impurity concentrations. This implies that the problem is multidimensional; several impurities are involved simultaneously. Therefore, we applied a statistical model, using the software package Cornerstone.

In the case of Oxygen, the LeTID amplitude is very low as long as  $c[\text{O}_i] < c_{\text{crit}}[\text{O}_i] = 10 \times 10^{17} \text{ cm}^{-3}$ . Above this value, the LeTID behavior in many cases becomes very severe; efficiency losses up to 8%<sub>rel</sub> are observed. The shape of the data cloud implies a quadratic dependence of LeTID on the Oxygen concentration exceeding  $c_{\text{crit}}[\text{O}_i]$ . In one crystal growth experiment (Growth Run 14), very high Aluminium concentrations occurred already in section A, up to  $4 \times 10^{14} \text{ cm}^{-3}$ . This crystal shows the strongest LeTID amplitudes in section A found in our investigations. In addition to Oxygen and Aluminium, there is also a clear trend to higher LeTID amplitudes for increasing Carbon concentrations.

In order to separate the contributions of Oxygen, Aluminium and Carbon, we modelled the LeTID amplitude as a linear combination of contributions from all impurity concentrations. However, for Oxygen we used as input parameter the square of the concentration exceeding  $c_{\text{crit}}[\text{O}_i]$ . We found a statistically significant correlation only for these three input parameters, while the contributions of the other metal contaminants or of Boron were statistically insignificant (Fig. 10).

This result can be visualized using so-called adjusted response graphs. In such graphs, the best fit to the linear model above is employed. The output parameter (in our case the efficiency relative to the initial value after one week of illumination) is plotted versus all input

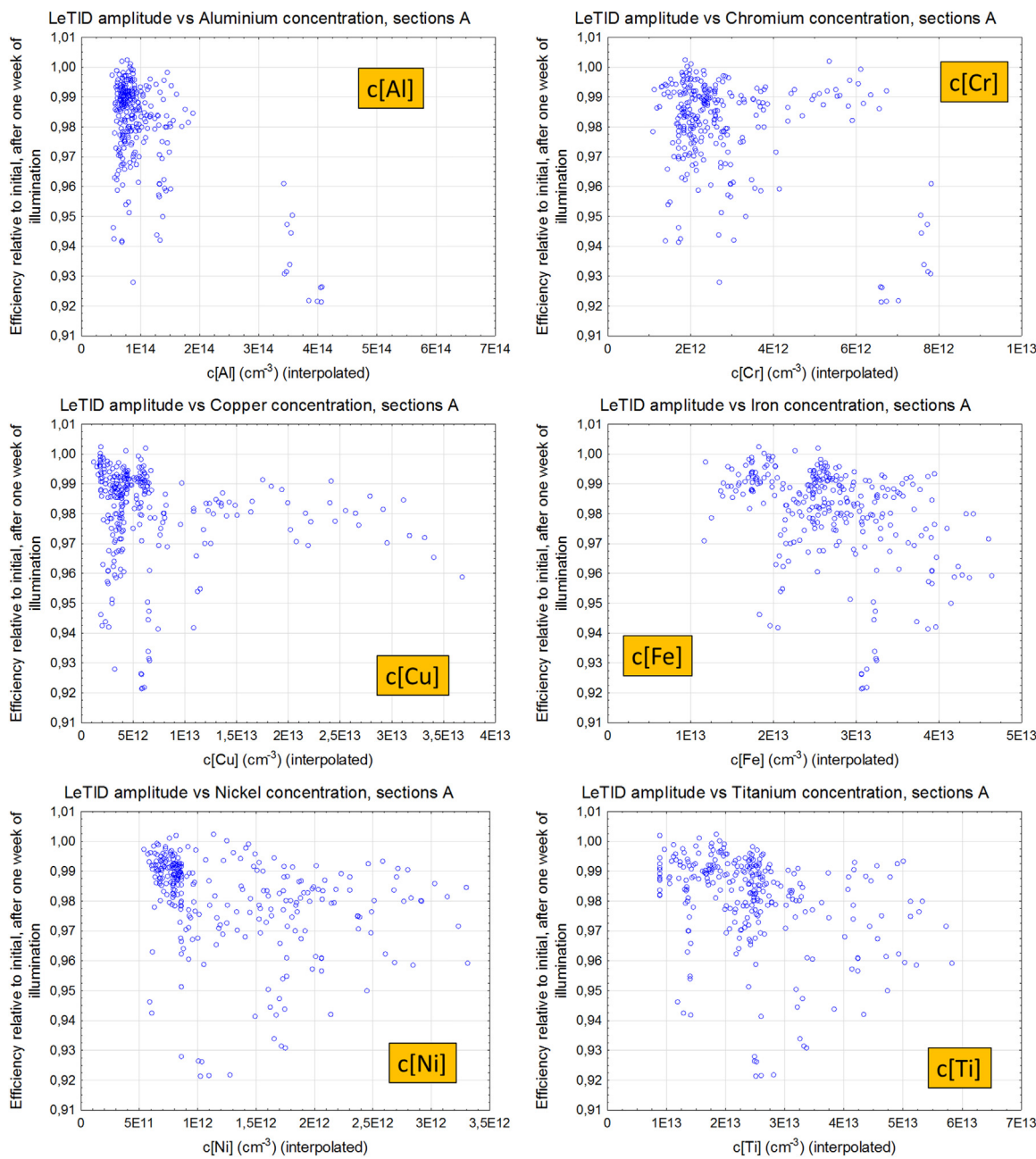


**Fig. 9.** Correlation of the LeTID amplitude (degradation amplitude after one week at (75 °C, 0.5 suns)) to the concentration of Al, Cr, Cu, Fe, Ni and Ti in the sections A of our crystals.

parameters separately; however, the value of the output parameter for each data point when plotted versus one particular input parameter is re-calculated in such a way as if all other input parameters had their mean value (Fig. 10 left). The relevant output parameters are chosen based on a test for statistical significance. In our case, such statistical significance is only found for Carbon concentration  $c[C_s]$ , Aluminium concentration  $c[Al]$  and transformed Oxygen concentration  $O_i$  transform ( $(c[O_i] - c_{crit}[O_i])^2$ ). These are marked in green in Fig. 10 right.

As shown above, there is an apparent trend to higher LeTID amplitudes even for the other metallic impurities. The reason is a weak cross correlation of these elements to Aluminium. Most likely there is a common source for a large part of the contamination concentrations somewhere in the growth process.

### 3.3.2. Results from section D (close to the tail)

In Figs. 11 and 12, the LeTID amplitude is shown in dependence of

the interpolated impurity concentrations as described above for solar cells originating from section D of our experimental crystals. In this part of the crystals, the Oxygen concentration is always well below the critical concentration of  $c_{crit} = 10 * 10^{17} \text{ cm}^{-3}$  found above in the top sections. Therefore, the LeTID amplitude in this part of the crystals is completely independent of the Oxygen concentration. No correlation is found either to the Boron concentration or base resistivity (Fig. 11). Closer to the tail, the LeTID effect becomes more pronounced; there both the Carbon and the Aluminium concentrations increase (Fig. 6). The apparent dependency of the LeTID amplitude on  $c[C_s]$  may, therefore, be due to cross correlation of both concentrations.

For the relevant metal impurities Fe, Cr, Cu, Ni and Ti, there is a general trend to larger LeTID amplitudes for higher concentrations. However, there are major deviations from a linear or otherwise continuous dependency. Contrary to that, the correlation to Aluminium is apparent.

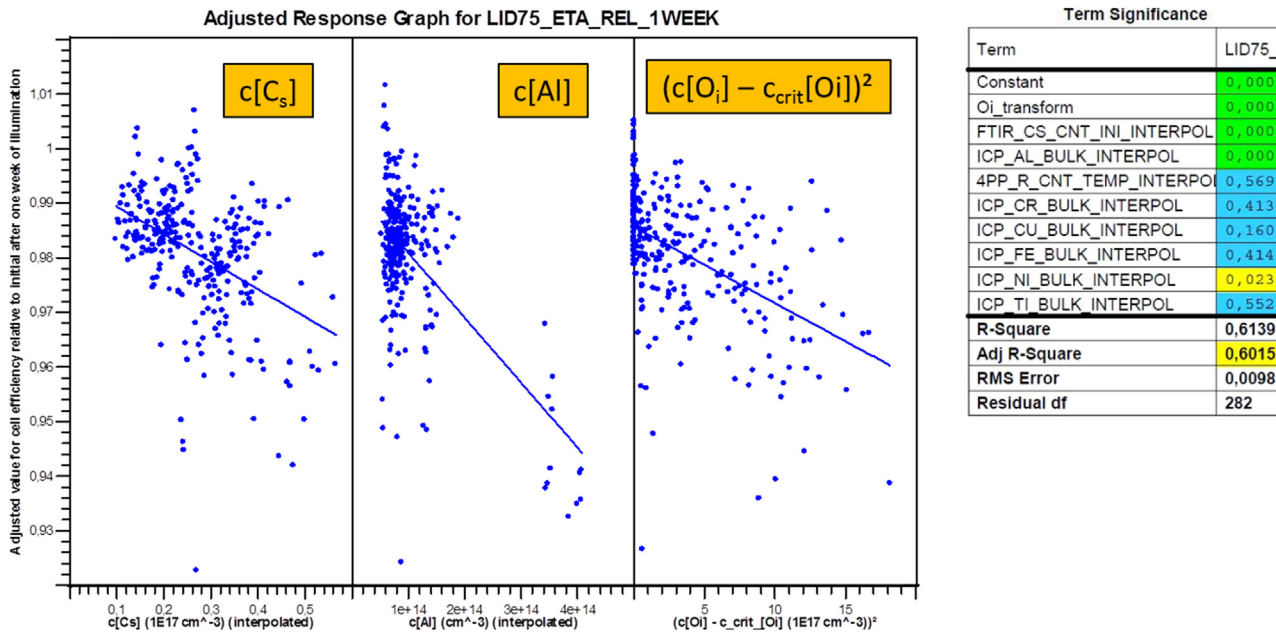


**Fig. 10.** Adjusted response graph for the LeTID amplitude (efficiency relative to initial after one week of illumination) for cells from section A with the significant input parameters Carbon concentration  $c[C_s]$ , Aluminium concentration  $c[Al]$  and transformed Oxygen concentration  $Oi_{transform}$   $((c[O_i] - c_{crit}[O_i])^2)$  (left). Result of the regression (right): Significant contributions are marked green, no statistically significant contribution is found for the other metallic contaminants.

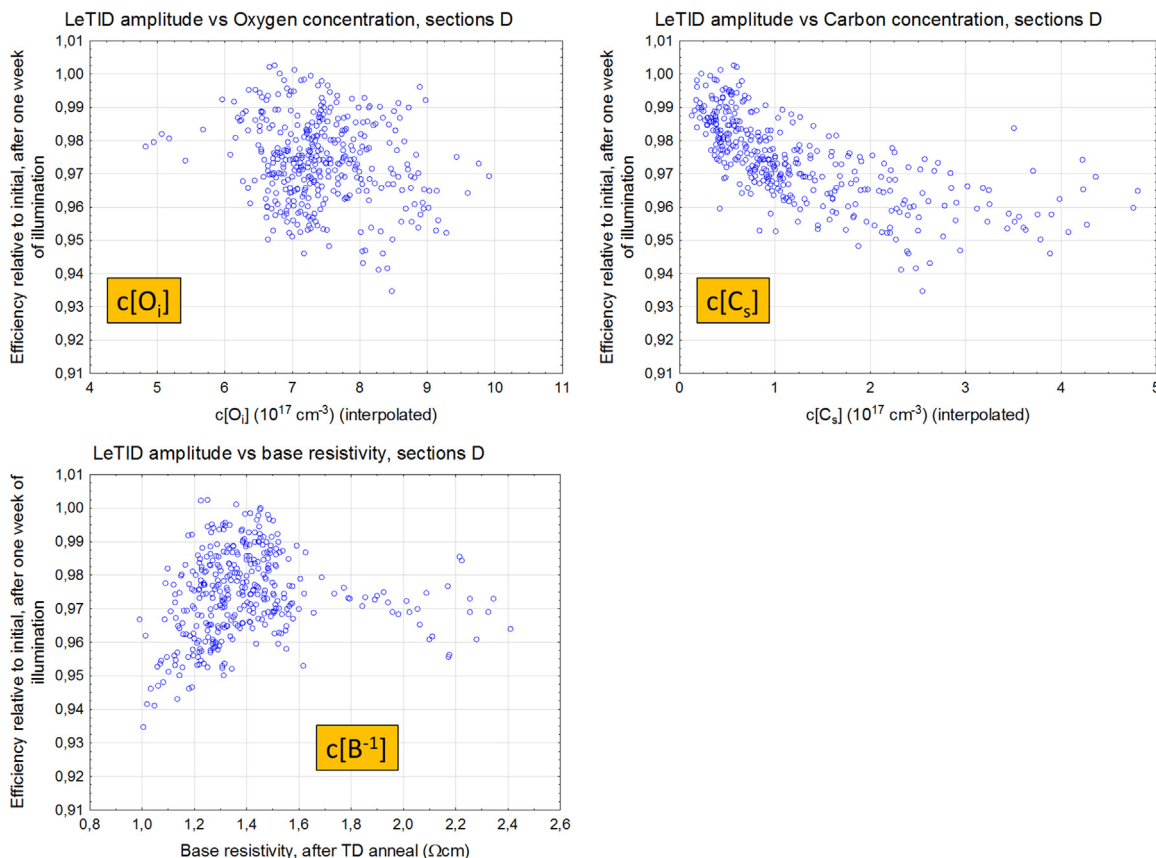


**Fig. 11.** Correlation of the LeTID amplitude (degradation amplitude after one week at  $(75^\circ\text{C}, 0.5 \text{ suns})$ ) for cells from section D to the concentration of Oxygen and Carbon, and to the base resistivity.

Modelling the LeTID amplitude as a linear combination of contributions from all impurity concentrations, we found a statistically significant correlation only for Aluminium, with a possible minor contribution from Carbon. In fact, the crystal of Growth Run 14, with its

very strong LeTID behavior (Fig. 4) showed only slightly increased Carbon concentrations along the crystal length. Also the concentrations of Oxygen and of the relevant metallic impurities were in the usual range. The Aluminium concentration, on the other hand, was

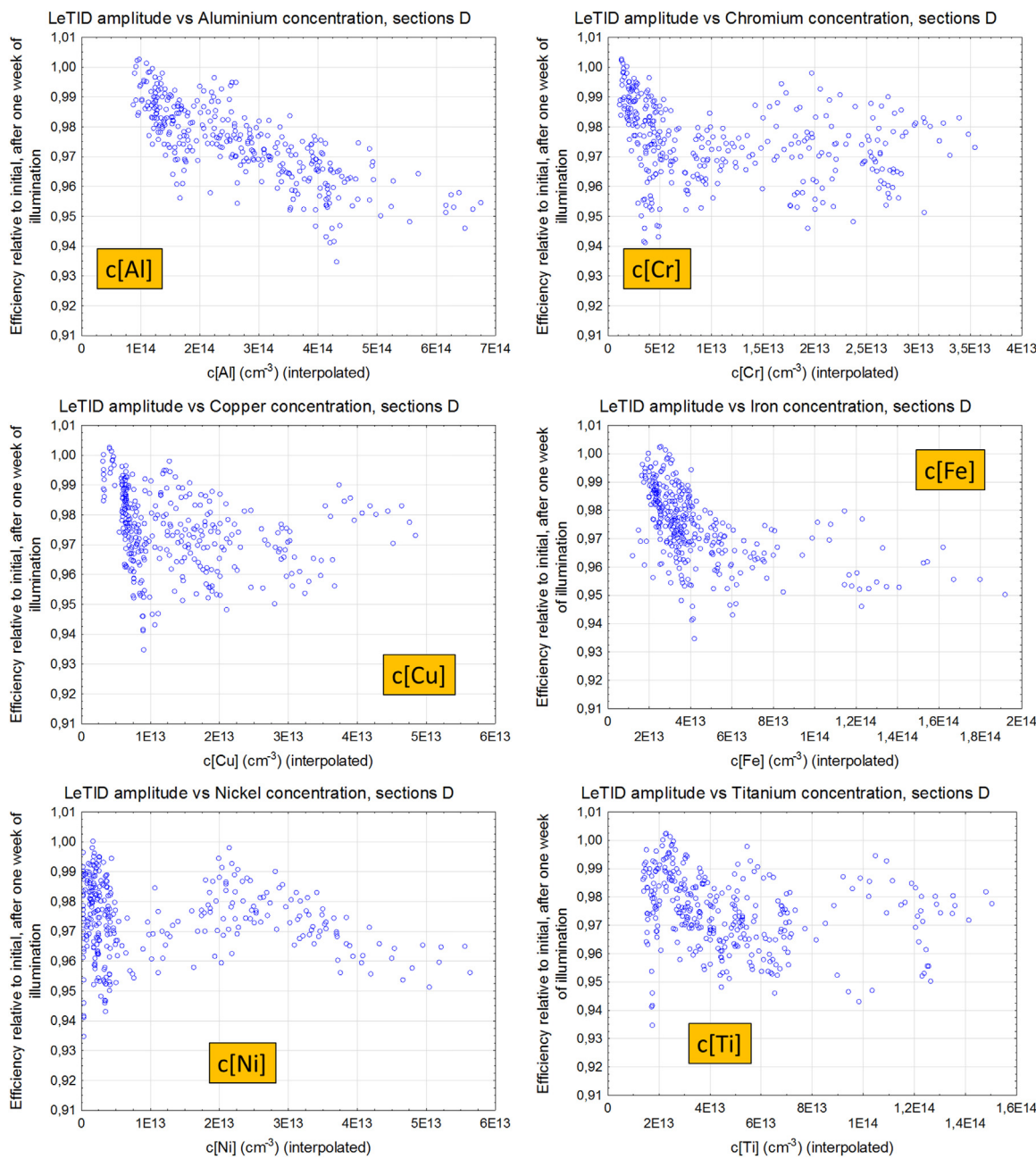


**Fig. 12.** Correlation of the LeTID amplitude (degradation amplitude after one week at (75 °C, 0.5 suns)) for cells from section D to the concentration of Al, Cr, Cu, Fe, Ni and Ti.

significantly higher than usual already in section A, which most likely explains the severe LeTID along the entire crystal length in this case.

#### 3.4. Effect of oxygen precipitation

##### 3.4.1. Annealing step prior to $\text{POCl}_3$ diffusion

Oxygen precipitation during cell processing is most likely to occur during the high temperature process steps, i.e. the  $\text{POCl}_3$  diffusion and the emitter oxidation. We tried to enhance this precipitation by adding an additional annealing step prior to the  $\text{POCl}_3$  diffusion since, according to literature, this should lead to the nucleation of seeds. After the annealing, cell processing for wafers from all groups continued in one batch.

Fig. 13 shows degradation curves for cells which received the various annealing steps. As mentioned above, these wafers were known to be partially affected by LeTID even in the standard process. The shape

of the degradation curve for the standard process (without additional annealing) is similar to the “mixed case” discussed above.

When wafers were annealed for a long time (180 min) at either 600 °C or 850 °C, the degradation behavior changes drastically. These cells are now completely LeTID dominated.

Photoluminescence (PL) images were recorded prior to and after the degradation cycle (Fig. 14). Long annealing at 600 °C or 850 °C (not shown) leads to formation of circular patterns of reduced minority carrier lifetime. Such features have been observed before and associated to Oxygen precipitates [18]. After one week of degradation at (75 °C; 0.5 suns), the rings become more pronounced. They are even visible weakly in the cells annealed for only 30 min at 600 °C after degradation.

No additional Oxygen precipitates can form during the degradation since the cell temperature is far too low. Thus, the lower PL intensity must be due to either enhanced recombination strength of the Oxygen precipitates themselves or to the formation of additional strong

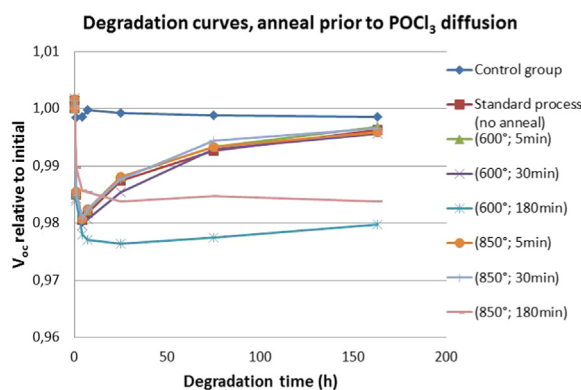


**Fig. 13.** Degradation curves for PERC solar cells which received an additional annealing step prior to  $\text{POCl}_3$  diffusion.

recombination centers in the vicinity of the precipitates.

#### 3.4.2. Variation of temperature ramp speeds

As discussed above, Oxygen precipitation is influenced by the details of the time-temperature curve during high temperature processing. In order to keep processing times short in industrial cell processing, heating up to process temperatures in  $\text{POCl}_3$  diffusion and emitter oxidation is done as quickly as the hardware allows. The same is true for ramping down. In our experiments, we intentionally chose ramp-up and ramp-down speeds four times slower than in the standard process.

The strongest effect in these process variations was found for the case in which the ramp-up speed to processing temperature for emitter oxidation was decreased. Fig. 15 shows the degradation curves for the standard process (left) and the “Slow ramp-up to oxidation” for three types of wafers with different Oxygen concentrations.

In cells made of wafers with low Oxygen concentration ( $(7\text{-}9)\times 10^{17} \text{ cm}^{-3}$ ), the degradation curves are B-O LID dominated in both process variations. For medium Oxygen concentration ( $(9\text{-}11)\times 10^{17} \text{ cm}^{-3}$ ), degradation is B-O LID dominated in the standard process, but of mixed type (B-O LID and LeTID) when the ramp-up speed is reduced. Cells

with high Oxygen concentration ( $(11\text{-}13)\times 10^{17} \text{ cm}^{-3}$ ) already contain a large LeTID contribution in the standard process, but are completely LeTID dominated in the process variation with slow ramp-up to oxidation.

## 4. Discussion

### 4.1. Summary of the experimental results

The LeTID amplitude in section D of the crystals is completely independent of the Oxygen and Boron concentration, proving again that LeTID is different from the B-O LID. Changing the Voronkov coefficient had no reproducible impact on the LeTID behavior.

A strong correlation was found between the LeTID amplitude and the concentration of Aluminium both close to the top and close to the tail in the grown crystals. A test for statistical significance showed that the apparent correlation to other relevant metallic impurities is probably due to a cross correlation to Aluminium.

In the top sections A, the Oxygen concentration often exceeds a critical value  $c_{\text{crit}} = 10^{17} \text{ cm}^{-3}$ . Above this value, the LeTID amplitude depends linearly on the Carbon and Aluminium concentrations and quadratically on the Oxygen concentration exceeding  $c_{\text{crit}}$ .

Process variations promoting the formation of Oxygen precipitates change the degradation behavior. Whenever Oxygen precipitates are formed in significant concentration during cell processing, the degradation becomes LeTID dominated.

### 4.2. Defect model

Even though LeTID and B-O LID are clearly due to different defects, their general behavior has similar features:

- Both are activated by excess minority charge carriers introduced into the material by illumination or forward biasing;
- Degradation becomes faster at moderately increased temperature;
- At even higher temperatures and presence of large concentrations of excess minority charge carriers, a regeneration process sets in.

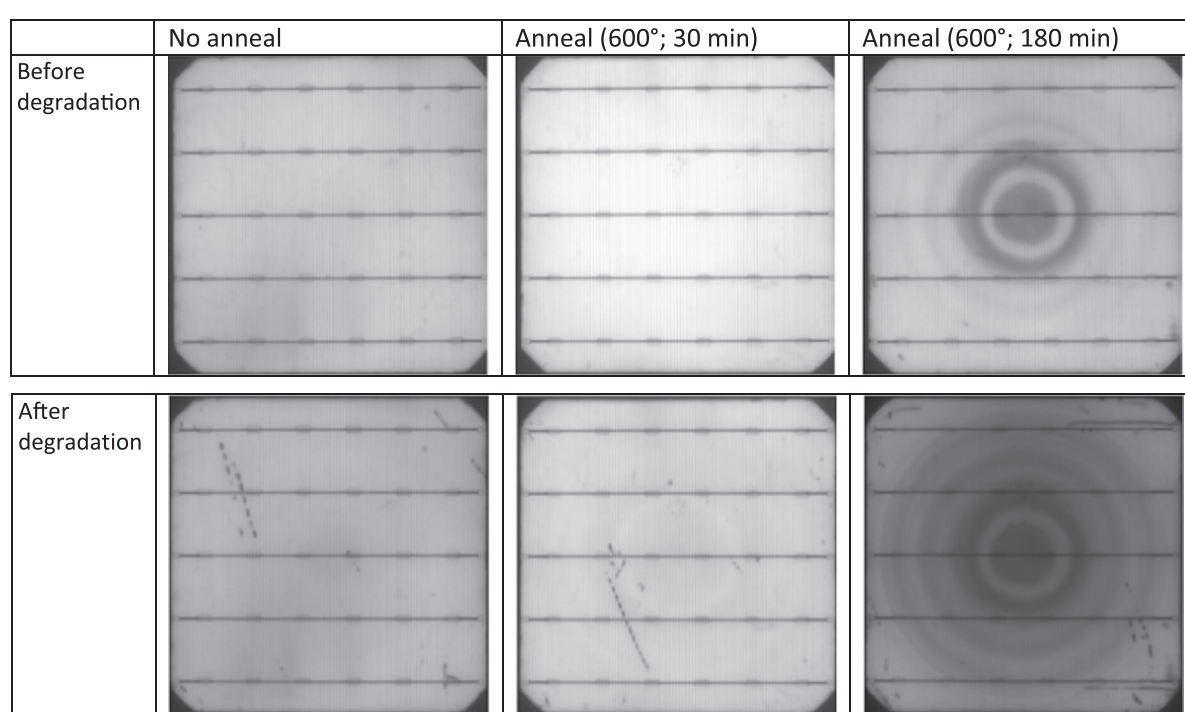


**Fig. 14.** Photoluminescence (PL) images recorded prior to and after degradation for one week.

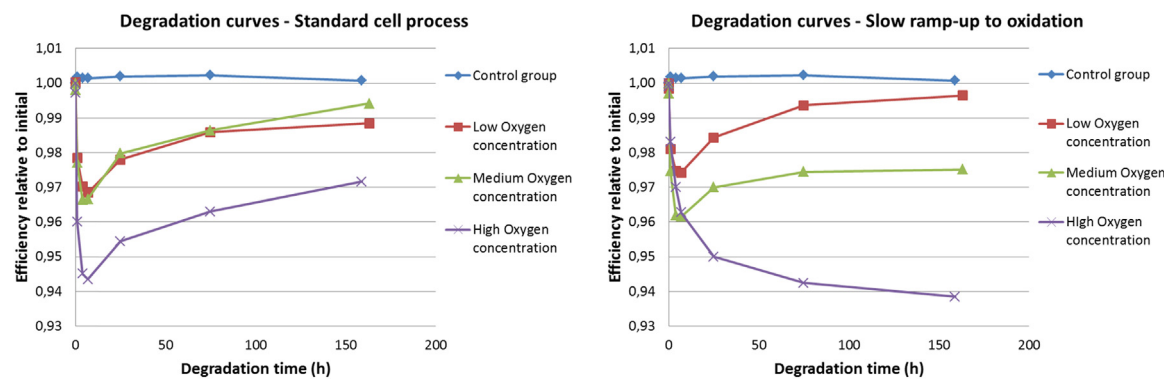


**Fig. 15.** Degradation curves for PERC solar cells produced from wafers with different Oxygen concentration processed using the standard process (left) and using a process variant with slower ramp-up speed to processing temperature in emitter oxidation (right).

The B-O LID has been reported to correlate to the concentration of Boron, while the LeTID amplitude, according to our results, is closely linked to the Aluminium concentration. Both Boron and Aluminium are acceptors in Silicon crystals and have similar electronic configuration. It is, therefore, likely that they form complex defects with similar defect properties.

Möller and Lauer suggested that all single acceptors in Silicon, i.e. Aluminium, Boron and Indium, with the exception of Gallium, can form a complex defect involving a Silicon interstitial atom in the close vicinity. This kind of defect was therefore called an  $A_{Si}-Si_i$  defect, with "A" representing the acceptor atom. In another paper the authors showed degradation data of Silicon crystals intentionally doped with Aluminium, Boron, Gallium and Indium [19]. No light induced degradation was found in Ga-doped material, while the B- and In-doped material degraded severely under illumination. It is well-known that Aluminium introduces a deep defect which strongly limits the minority carrier lifetime [20]. Therefore, the starting value of the minority carrier lifetime in the crystal doped with  $\sim 4 \times 10^{15} \text{ cm}^{-3}$  Aluminium atoms was already limited to approximately 18  $\mu\text{s}$ . Nevertheless, there was a clear light induced degradation which seems to occur on a longer time scale than the LID in the B- and In-doped crystals.

In our crystals, the Aluminium concentration is at least one order of magnitude lower, even in the crystals with highest Aluminium contamination. Therefore, the minority carrier lifetime prior to illumination is sufficiently high not to limit the cell efficiency significantly. However, under illumination a strongly recombination active defect related to Aluminium is formed.

The experiments with process variants which enhance Oxygen precipitation clearly prove that the LeTID amplitude increases strongly when such precipitates are formed. In cells processed with the standard process, the LeTID amplitude depends superlinearly on the Oxygen concentration exceeding a critical value of  $c_{crit} = 10 \times 10^{17} \text{ cm}^{-3}$ . The statistical model used a quadratic dependence. However, the scatter in the data is relatively large. A fit using exponents varying from the chosen value of 2 would lead to a similarly consistent result.

This quadratic or nearly-quadratic dependence of the LeTID amplitude on the excess Oxygen concentration does not necessarily mean that Oxygen is a constituent of the defect responsible for LeTID. Since the growing Oxygen precipitate requires space in the Silicon lattice, neighboring Silicon lattice atoms have to be displaced and are ejected as Silicon interstitials. Oxygen precipitation, thus, increases the (local) concentration of this intrinsic defect, which becomes available for formation of complex defects. During the high temperature process steps ( $\text{POCl}_3$  diffusion, emitter oxidation, fast firing), the Silicon interstitials may be sufficiently mobile to diffuse to Aluminium atoms nearby.

The effect of Carbon on the LeTID amplitude may be even more indirect. There are reports that Carbon influences Oxygen precipitation, e.g. by providing additional nucleation sites. Increasing the Carbon

concentration may, thus, lead to more efficient Oxygen precipitation which, in turn, produces additional Silicon interstitials.

Studies published recently discuss a direct involvement of Hydrogen in the LeTID effect. Our results do not support the idea that Hydrogen in elemental form or as small clusters is directly responsible for LeTID, since all of our cells can be expected to contain very similar amounts of Hydrogen. In wafers containing low Oxygen and Aluminium concentrations, such cells do not suffer from LeTID. The observed dependence of LeTID on Hydrogen may, thus, be a more indirect one. In the presence of Hydrogen, the diffusivity of other contaminants, e.g. Oxygen species has been shown to be increased. If this is true, the formation of precursors of the LeTID defect may be enhanced by Hydrogen.

No microscopic identification of the defect responsible for the LeTID effect is possible based on our observations. There are, however, indications that the  $Al_{Si}-Si_i$  configuration may be a good candidate for this defect.

## 5. Conclusions

We repeatedly and reproducibly find increased LeTID amplitudes in tail parts of experimental Cz crystals. The effect increases in the 2nd and 3rd pull from identical crucibles compared to the 1st pull. The position of the raw Silicon wafers was randomized prior to and during the cell processing. It can, therefore, be ruled out that LeTID originates from cell processing only. There has to be a contribution of defect(s) already present after crystal growth. The LeTID amplitude increases strongly whenever Oxygen precipitation occurs during cell processing. This is often the case for wafers originating very close to the seed, since the Oxygen concentration there may be high enough to lead to Oxygen precipitation in the standard process. Process variations promoting the precipitation process enhance the LeTID effect.

The concentration of the relevant impurities was determined at four positions along the crystal length. From linear interpolation, we could assign impurity concentration values to each individual solar cell. The LeTID amplitude was found to be completely independent of the Boron concentration and to the Oxygen concentration as long as it does not exceed a critical value of  $c_{crit}[O] \sim 10 \times 10^{17} \text{ cm}^{-3}$ . It is, on the other hand, strongly correlated to the Aluminium concentration. In order to avoid LeTID, an Aluminium concentration of  $1 \times 10^{14} \text{ cm}^{-3}$  should not be exceeded and Oxygen precipitation in the cell process should be avoided.

While no exact configuration of the defect responsible can be extracted from our data, the results can be consistently interpreted assuming the  $Al_{Si}-Si_i$  configuration.

## Appendix A. Supporting information

Supplementary data associated with this article can be found in the

online version at [doi:10.1016/j.solmat.2018.06.009](https://doi.org/10.1016/j.solmat.2018.06.009).

## References

- [1] M. Müller, G. Fischer, B. Bitnar, S. Steckemetz, R. Schiepe, M. Mühlbauer, R. Köhler, P. Richter, C. Kusterer, A. Oehlke, E. Schneiderlöchner, H. Sträter, F. Wolny, M. Wagner, P. Palinginis, D.H. Neuhaus, Loss Analysis of 22% efficient industrial PERC solar cells, in: Proceedings of the 7th International Conference on Silicon Photovoltaics, SiliconPV 2017, Energy Procedia Vol. 124, p. 131.
- [2] F. Ye, W. Deng, W. Guo, R. Liu, D. Chen, Y. Chen, Y. Yang, N. Yuan, J. Ding, Z. Feng, 22.13% Efficient Industrial p-Type Mono PERC Solar Cell, in: Proceedings of the 43rd IEEE Photovoltaic Specialist Conference, p. 3360.
- [3] H. Fischer, W. Pschunder, Investigation of photon and thermal induced changes in silicon solar cells, in: Proceedings of the 10th IEEE Photovoltaic Specialists Conference, p. 404.
- [4] J. Schmidt, K. Bothe, Structure and transformation of the metastable boron- and oxygen-related defect center in crystalline silicon, Phys. Rev. B 69 (2004) 024107.
- [5] C. Möller, K. Lauer, Light-induced degradation in indium-doped silicon, Phys. Status Solidi RRL 7 (2013) 461.
- [6] M. Hakala, M.J. Puska, R.M. Nieminen, First-principles calculations of interstitial boron in silicon, Phys. Rev. B 61 (2000) 8155.
- [7] K. Ramspeck, S. Zimmermann, H. Nagel, A. Metz, Y. Gassenbauer, B. Birkmann, A. Seidl, Light induced degradation of rear passivated mc-Si solar cells, in: Proceedings of the 27th European Photovoltaic Solar Energy Conference, Vol. 1, p. 861.
- [8] F. Kersten, P. Engelhart, H.-C. Ploigt, F. Stenzel, K. Petter, T. Lindner, A. Szpath, M. Bartzsch, A. Stekolnikov, M. Scherff, J. Heitmann, J.W. Müller, A new light induced volume degradation effect of mc-Si solar cells and modules, in: Proceedings of the 31st European Photovoltaic Solar Energy Conference, 2015, p. 1822.
- [9] F. Fertig, R. Lantzsch, A. Mohr, M. Schaper, M. Bartzsch, D. Wissen, F. Kersten, A. Mette, S. Peters, A. Eidner, J. Cieslak, K. Duncker, M. Junghänel, E. Jarzembski, M. Kauert, B. Faulwetter-Quandt, D. Meißner, B. Reiche, S. Geißler, S. Hörlein, C. Klenke, L. Niebergall, A. Schömann, A. Weihrauch, F. Stenzel, A. Hofmann, T. Rudolph, A. Schwabedissen, M. Gundermann, M. Fischer, J.W. Müller, D.J.W. Jeong, Mass production of p-type Cz silicon solar cells approaching average stable conversion efficiencies of 22%, in: Proceedings of the 7th International Conference on Silicon Photovoltaics, SiliconPV 2017, Energy Procedia 124 338.
- [10] F. Kersten, J. Heitmann, J.W. Müller, Influence of  $\text{Al}_2\text{O}_3$  and  $\text{SiN}_x$  passivation layers on LeTID, in: Proceedings of the 6th International Conference on Silicon Photovoltaics, SiliconPV 2016, Energy Procedia 92 828.
- [11] C. Vargas, K. Kim, G. Coletti, D. Payne, C. Chan, S. Wenham, Z. Hameiri, Influence of silicon nitride and its hydrogen content on carrier-induced degradation in multicrystalline silicon, in: Proceedings of the 33rd European Photovoltaic Solar Energy Conference and Exhibition 2016, p. 2015.
- [12] A.E. Morishige, M.A. Jensen, D.B. Needelman, K. Nakayashiki, J. Hofstetter, T.T.A. Li, T. Buonassisi, Lifetime spectroscopy investigation of light-induced degradation in p-type multicrystalline silicon PERC, IEEE J. Photovolt. 6 (2016) 1466.
- [13] T. Niewelt, F. Schindler, W. Kwapił, R. Eberle, J. Schön, M.C. Schubert, Understanding the light-induced degradation at elevated temperatures: similarities between multicrystalline and floatzone p-type silicon, Prog. Photovolt. Res. Appl. (2017) 1, <https://doi.org/10.1002/pip.2954>.
- [14] R. Eberle, W. Kwapił, F. Schindler, M.C. Schubert, S.W. Glunz, Impact of the firing temperature profile on light induced degradation of multicrystalline silicon, Phys. Status Solidi RRL 10 (2016) 861.
- [15] V.V. Voronkov, R. Falster, Vacancy and self-interstitial concentration incorporated into growing silicon crystals, J. Appl. Phys. 86 (1999) 5975.
- [16] A. Herguth, G. Schubert, M. Kaes, G. Hahn, Avoiding boron-oxygen related degradation in highly boron doped Cz silicon, in: Proceedings of the 21st European Photovoltaic Solar Energy Conference, p. 530.
- [17] A. Borghesi, B. Pivac, A. Sassella, A. Stella, Oxygen precipitation in silicon, Appl. Phys. Lett. 77 (1995) 4169.
- [18] J. Haunschild, J. Broisch, I. Reis, S. Rein, Cz-Si wafers in solar cell production: efficiency-limiting defects and material quality control, Photovolt. Int. J. (2012) 50 (50ª edição).
- [19] C. Möller, K. Lauer,  $\text{As}_i\text{-Si}_i$ -defect model of light-induced degradation in silicon, in: Proceedings of the 4th International Conference on Silicon Photovoltaics, SiliconPV 2014, Energy Procedia Vol. 55, p. 559.
- [20] J. Schmidt, N. Thiemann, R. Bock, R. Brendel, Recombination lifetimes in highly aluminum-doped silicon, J. Appl. Phys. 106 (2009) 093707.